Probing the D-region ionosphere globally with Earth Networks Total Lightning Network data

Lay, Erin Hoffmann
Hudson, Emily Rose
Markowski, Danielle Giuseppa
Shao, Xuan-Min
Anderson, Todd Shelby

To be published in: Advances in Space Research

DOI to publisher's version: 10.1016/j.asr.2024.09.049

Journal Pre-proofs

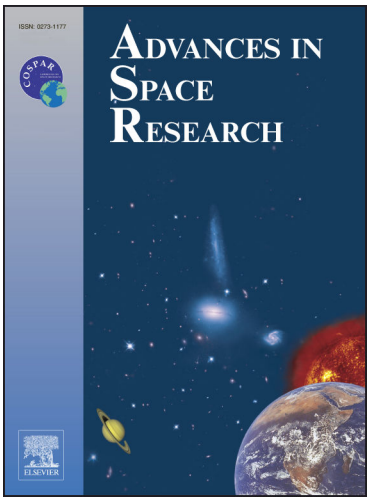

Probing the D-region ionosphere globally with Earth Networks Total Lightning Network data

Erin Lay, Emily Hudson, Danielle Markowski, Xuan-Min Shao, Todd Anderson

PII: S0273-1177(24)00983-9
DOI: https://doi.org/10.1016/j.asr.2024.09.049
Reference: JASR 17819

To appear in: *Advances in Space Research*

Received Date: 31 May 2024
Revised Date: 19 September 2024
Accepted Date: 24 September 2024

Please cite this article as: Lay, E., Hudson, E., Markowski, D., Shao, X-M., Anderson, T., Probing the D-region ionosphere globally with Earth Networks Total Lightning Network data, *Advances in Space Research* (2024), doi: https://doi.org/10.1016/j.asr.2024.09.049

Probing the D-region ionosphere globally with Earth Networks Total Lightning Network data

Erin Lay[1], Emily Hudson[1], Danielle Markowski[1], Xuan-Min Shao[1], Todd Anderson[1]

1) Los Alamos National Laboratory, Los Alamos, NM 87545, U.S.A.

Abstract:

An existing technique to use broadband lightning waveforms to probe the D-region ionosphere (60-90 km altitude) is shown to be extendable to a global scale using the Earth Networks Total Lightning Network (ENTLN). This paper demonstrates the technique in detail on a region of the Southeastern United States. This demonstration shows that diurnal D-region height variation and smaller time-scale variations on the order of tens of minutes to hours are evident in the measurement. The technique is then extended to three additional global regions on this same day: Northeastern U.S., India, and Japan. The diurnal behavior between these different regions is compared to a D-region model from the International Reference Ionosphere.

Key Words

D-region ionosphere, VLF/LF remote sensing, global ionosphere

1. Introduction

The ionosphere is an ionized plasma from about 60 – 2000 km above the Earth. It affects radio signals traveling through it from ground-to-satellite and those reflected below it, such as low-frequency (LF; 30-300kHz) and very-low-frequency (VLF; 3-30 kHz) signals. The lower boundary of the ionosphere is called the D-region, typically defined as the region between 60-90 km altitude. The profile of this region varies significantly between day and night, mainly due to changes in solar flux. The altitude of the layer decreases during the daytime and increases at night, causing major variation in the frequencies and distances that signals can propagate (Kelley, 2009; Schunk and Nagy, 2000). It has long been known that strong solar flares can also impact the polar ionosphere, causing significant radio blackouts that are problematic for transpolar flights (Dellinger, 1937; Frissell et al., 2019). More recently, studies have shown that smaller temporal and spatial scale variations in the ionosphere can be caused by events on the ground, such as thunderstorms, hurricanes, earthquakes, volcanos, and explosions (Galvan et al., 2012; Lay et al., 2015; Lay, 2018; Astafyeva, 2019). More specifically, recent studies have shown effects on the D-region ionosphere related to thunderstorms and hurricanes (Lay and Shao, 2011a,b; Marshall and Snively, 2014).

While these D-region variations can have significant effects on subionospheric radio propagation, they are very difficult to measure via remote sensing due to the low electron density in the D-region (typically $10^6 – 10^9$ electrons/m^3). Several hundred rocket flights over the past 80 years have sporadically measured the electron density *in situ* and been collated into a semi-empirical model of the global D-region variability called the Faraday-International Reference Ionosphere (FIRI) (Friedrich et al., 2018; Friedrich and Torkar, 2001). The International Reference Ionosphere (IRI) (Bilitza et al., 2022) includes the FIRI as a standalone electron density model, but the default D-region electron density that is merged with the upper ionosphere is based on even fewer rocket measurements. These D-region models have very little data available for validation. We use the default IRI 2016 D-region model for comparison to measurements later in this paper.

Powerful VLF transmitters have been used for decades to measure the average behavior of the lower ionosphere over long (100s-1000s km) great circle paths (e.g., Wait and Spies, 1964; Ferguson, 1980; Thomson, 1993). More recent studies have begun to use these transmitters to probe the ionosphere at finer temporal and spatial scales (Cohen et al., 2018). However, because VLF transmitters require significant power to produce VLF radio signals, the transmitters are limited in number and location. Other recent studies have begun using naturally-generated lightning signals detected in the VLF to LF to study the D-region ionosphere (Cummer et al., 1998; Cheng et al., 2007; Lay et al., 2011a,b; Shao et al., 2013, McCormick et al., 2018). The advantage to this type of approach is that lightning emits strongly in the VLF, providing a powerful signal to detect with relatively inexpensive receivers. Lightning occurs globally, so this technique can be expanded to a larger scale depending on the availability of LF/VLF receivers. The expansion of the LF/VLF lightning probing technique to global scales is the focus of this paper.

A recent technique has demonstrated the utility of broadband LF/VLF time-domain waveforms, detected 300 – 900 km away from RF receivers, to probe the D-region ionosphere with high temporal and spatial resolution (Lay et al. 2011a,b; 2014). This technique used signals from the Los Alamos Sferic Array (LASA) that was deployed in the U.S. Great Plains in 2005 – 2006. In order to expand the technique to a global scale, a global network of sensors that records LF/VLF waveforms and locates the associated lightning strokes is required. These sensors detected the direct ground wave of the LF/VLF lightning signal followed by the ionospheric reflection of the signal (Figure 1a). In this paper, we demonstrate that the existing Earth Networks Total Lightning Network (ENTLN) can be used for this technique (Liu and Heckman, 2011; Zhu et al., 2017, DiGangi et al., 2022) to observe both large-scale diurnal variability and small-scale ionospheric variations consistent with gravity wave time scales.

2. Data Processing

The ENTLN consists of more than 1500 lightning sensors globally. Lightning signals detected by these sensors are located by a time-of-arrival minimization technique (Liu and Heckman, 2011; Zhu et al., 2017), and the signals at each station are recorded and saved in a compressed format. The compressed format only saves data points when the change in measured digitizer counts surpasses a threshold. Because of that, the data are more highly sampled in time near peaks and troughs of the signal. Figure 1b shows an example of the measured digitizer counts of a compressed signal from an ENTLN receiver as black points. The example waveform in Figure 1b arises from a negative cloud-to-ground (-CG) lightning stroke, as is required for the LF/VLF probing technique in (Lay et al, 2011a,b; 2014). Here we demonstrate the steps necessary to recover normalized electric-field waveforms from these compressed signals. These normalized waveforms are necessary to use the probing technique.

From the recorded digitized counts, we must recover the normalized electric field (E-field). The absolute value of the E-field is not important, only the relative amplitude values. We first interpolate this signal to a 1 μs time step (1b, solid line). We then account for the 32 μs characteristic time of the preamplifier circuit to convert measured digitizer voltage to electric field by the following equation:

$$\frac{AdE(t)}{dt\,\varepsilon_0} = C\frac{ds(t)}{dt} + \frac{s(t)}{R} = \left(RC\,\frac{ds(t)}{dt} + s(t)\right)/R, \text{ (Eqn. 1)}$$

where *A* is the effective area of the receiver plate, $\mathcal{E}_0$ is the permittivity of free space, *C* is the capacitance, *R* is the resistance, *E(t)* is the electric field, and *s(t)* is the measured signal voltage. Solving for *E(t),* we get a relative electric field of:

$$E(t) \propto \tau s(t) + \int s(t)dt \text{ , (Eqn. 2)}$$

where $\tau = RC$ = 32 μs. Figure 1c shows the resulting normalized waveform. The waveform shows a groundwave from the lightning stroke as well as the ionospheric reflection peak later in time. The relationship between these two features provides information about the ionosphere, namely the time difference between the groundwave and ionospheric reflection (Δt) and the ratio of the peak magnitudes (peak magnitude of ionospheric reflection/peak magnitude of ground wave = *R*). These are described in detail in Lay et al., 2014.

For this work, we limit the ENTLN data to only -CG lightning with peak current magnitude > 30 kA, as well as to lightning waveforms that are detected at receivers that are 300-900 km from the located lightning source. It is possible for the compressed ENTLN waveforms to lose too much important information in the compression for them to be useful in this technique. Therefore, we require that there be at least N = 85 samples that span more than T = 150 μs after the ground wave. In addition, we require a density of points (N/T) in the entire waveform of at least 0.25 points/μs. These criteria allow for a more robust interpolation and conversion to electric field, as shown in Figure 1b&c. From each waveform that passes the criteria above, we measure Δt and R.

Figure 2a shows an example of -CG lightning (colored dots) detected and located in the Southeastern United States from 00:00 – 10:00 UTC on 1 May 2017 by ENTLN. The color bar represents UTC time of day. The local time of this region is UTC – 5, or 19:00 – 05:00 LT, indicating nighttime conditions for this measurement. The blue squares show ENTLN station locations. To demonstrate consistency with previous results (Shao and Jacobson, 2009), we use a subset of these lightning waveforms, detected at station PLMCH (Fig. 2a, red square). To limit the azimuthal direction of propagation and to limit changes in the ionosphere over time, we further reduce this data set to 00:00 – 02:00 UTC, with latitudes between 27° and 33°, and longitudes between -90° and -86°. These signals all propagate from southwest to northeast, with an azimuthal angle to the magnetic field of about 45°. We bin these waveforms by distance to station into 50-km bins and show a superposed epoch of waveform by distance from station in Figure 2b. The waveforms are offset on the y-axis by distance between event and station. The number of waveforms (N) used in each superposed epoch is shown on the righthand side of the plot. The behavior of waveform versus distance for a nighttime ionosphere is consistent with modeled results of Shao and Jacobson (2009), and with previous demonstrations of this technique using LASA waveforms (Lay et al., 2011a). This indicates that the ENTLN waveforms can be used in a similar manner as LASA waveforms to probe the D-region ionosphere.

3. Results

In this paper, we demonstrate this technique on a case study over a region with significant thunderstorms in the Southeastern U.S. on 01 May 2017. This region has good coverage by ENTLN stations (Figure 2a, blue squares), resulting in a high detection efficiency of lightning in the region, and a large number of stations at our required distances of 300-900 km from lightning strokes in the region.

First, we look at the diurnal behavior of the D-region ionosphere in this region. We bin the ENTLN waveforms detected by a single station into 1° latitude x 1° longitude x 5-min bins and create a superposed, normalized waveform in each bin, similar to those shown in Figure 2b. From each of these waveforms, we then measure Δt from the superposed waveform and convert to effective ionospheric height of the D-region using the simple spherical geometry depicted in Figure 1a. Effective ionospheric height, *h*, is calculated by (McDonald III et al., 1979, adapted from Laby et al., 1940):

$$h = R_e\left[\cos\left(\frac{r}{2R_e}\right) - 1\right] + \sqrt{\left(\frac{r+c\Delta t}{2}\right)^2 - \left(R_e \sin\left(\frac{r}{2R_e}\right)\right)^2}, \text{ (Eqn. 3)}$$

in which *r* is the distance between the center of the grid cell and the receiving station, R_e = 6371 km (mean radius of Earth), and *c* is the speed of light. This is a simple spherical approximation that accounts for the curvature of the Earth. It does not consider the fact that rays of the same frequency that enter the ionosphere at steeper angles (smaller *r*) will propagate higher in altitude before reflecting than waves reflecting at a more grazing angle (larger *r*). However, we are looking for the general behavior in this case, so we are willing to make this simplification. ENTLN location accuracy is reported to have a median accuracy of 250 m (Zhu et al., 2017), which affects the accuracy of the height calculation by less than 70 m.

We are interested in studying the diurnal variation of the measured D-region effective height using this method. Diurnal variation should be driven primarily by solar input, so we want to look at all locations at the same local solar time. The probed measurement locations (midpoints between all lightning and all stations) in this case study cover more than 1000 km x 1000 km. Thus, a measurement at a given universal time at one edge of the probed region (for example, 30°N, 90°W) could have significantly different local solar time than a measurement at the other side of the region (for example, 30°N, 80°W). For that reason, to understand the average diurnal behavior of this region, we convert measurements to local solar time:

$$LT = UT\_hours + 12\_hours\frac{longitude\_deg}{180\ deg}, \text{ (Eqn. 4).}$$

Figure 3 shows the estimated ionospheric height and its variation over local solar time as determined by this method. Below, we will look at smaller regions individually in universal time. The colored dots show the estimated averaged height at each grid cell. The colorbar represents *r*, the distance between lightning and station. One can see the slight effect of signals with shorter *r* penetrating higher into the ionosphere due to their steeper angle of incidence, but the effect is minimal and the overall diurnal trend is still apparent. The solid black line shows the median of all measurements in 30-min increments.

The measured heights represent effective reflection heights of the broadband signal. ENTLN receivers have a bandwidth of 1kHz to 10MHz. However, we interpolate the ENTLN irregularly-spaced time-domain measurements to a 1 μs cadence, which effectively reduces the upper end of the bandwidth to the Nyquist frequency of 500 kHz. In addition, lightning emits most strongly in the VLF, with power falling off as frequencies increase into the LF. For that reason, the majority of the broadband signal power falls into the 10-100kHz range, corresponding to electron densities of about 10^6 to 10^8 electrons/m^3. This is consistent with previous work on this D-region technique using lightning waveforms from the Los Alamos Sferic Array to probe the lower ionosphere (Lay et al., 2014). Next, we look at modeled plasma frequencies in altitude from the International Reference Ionosphere (IRI-2016, Bilitza et al., 2022) at a location of 30° latitude, -87° longitude. White squares in Figure 3 show the altitude at which the plasma frequency of the IRI matched a frequency of 100 kHz, from the general plasma frequency definition of $\omega_{pe}{}^2 = \frac{n_e e^2}{m_e \varepsilon_0}$. This frequency corresponds to an electron density value of 124 electrons/cm^3. Therefore, one can interpret the variation in white squares over time as the IRI prediction in the variation in height of where the electron density equals 124 electrons/cm^3. As we do not know *a priori* which electron density value corresponds to our measured effective height, we choose the IRI 100 kHz value as a benchmark as the upper end of the range of our waveform sensitivity. In addition, it is important to note that IRI is poorly sampled and extremely limited in validation at these altitudes. Therefore, we are not using IRI as "truth" in this comparison, rather we are using it for comparison purposes regarding magnitude and timing of diurnal variation.

Compared with our D-region measurements, we see that the IRI model gives the general diurnal trend in the variation of the D-region, but it misses quite a lot of detail. For example, the measured ionospheric height jumps rapidly to around 85 km at the beginning of the nighttime, as opposed to the slow rise predicted by IRI. Then it stays at this relatively flat peak for the duration of the night, with slight variation on the order of 2-4 km. The daytime IRI behavior seems to follow our measurements well, although there are large gaps in our measurements due to lack of lightning activity in the region at that time.

In addition to looking at the general diurnal trend with this technique, we also look at shorter time scale variation on the order of tens of minutes to hours. Figure 4a shows a map of probed ionospheric locations (gray dots) from 01:00 – 10:00 UT (local nighttime) on 1 May 2017, and six regions that we will look at in more detail (black boxes). The six regions are labeled numerically (1-6). The ionospheric height variation in each box is shown as two-dimensional (2D) histograms in Figures 4b-g. We choose to show the 2D histogram to convey information about how many lightning measurements are available for each height measurement. The color bar goes from dark blue (45 measurements per cell) to yellow (1 measurement per cell). We can see variation in median height of 1-4 km with time scales of 30 minutes to several hours in nearly all boxes. These time scales and magnitudes are consistent with previous studies of gravity wave activity over thunderstorms in the D-region ionosphere (Lay et al., 2011a, 2011b).

A substantial benefit of using ENTLN data for this technique is its global coverage. For that reason, we also looked at other regions of the globe for this same day. We found three additional regions with good lightning activity and station coverage during this day. These three regions, Northeastern U.S., India, and Japan, in addition to the entire day of data for the original Southeastern U.S. region, are shown in Figure 5. The thunderstorm system that caused significant lightning activity in the Southeastern U.S. also brought significant lightning throughout the day to the Northeastern United States. India had significant lightning activity, but fewer stations overall. The majority of the waveforms in the Indian region that meet criteria happened between 05:00 and 15:00 UTC, corresponding to 10:00 to 20:00 LT. While Japan had a very active thunderstorm occurring off the coast for much of the day, there are relatively few receivers in Japan, and lightning in the thunderstorm was often more than 900 km away from the receivers. The majority of good waveforms in the Japan region occurred between 03:00 and 08:00 UTC, corresponding to 12:00 to 17:00 LT. Although the Japanese and Indian regions were limited in coverage, they were able to fill in measurements during local daytime D-region conditions. Other regions with significant numbers of ENTLN stations did not have significant lightning activity on this day that met the required waveform criteria above, so we only look in-depth at these 4 regions. Future studies will choose other dates that could have different global coverage.

Figure 6 shows effective ionospheric height (gray dots) versus local time from 18:00 LT – 20:00 LT the next day for each of these four regions. 00:00 UT 1 May 2017 for the Northeastern U.S. (Fig. 6a) and Southeastern U.S. (Fig. 6b) is around 18:00 LT the previous evening. 00:00 UT in India is 05:00 LT (Fig. 6c), and 00:00 UT in Japan is 09:00 LT (Fig. 6d). India and Japan did not have significant lightning activity that was detected within 300-900 km of ENTLN stations after their respective 20:00 LT, which is why the local time axis is truncated at that point. The black line in each panel shows the median of the measurements in 30-minute bins. The blue squares are IRI-predicted heights where the plasma frequency equals 100 kHz. The location of the IRI modeling run for each region is shown as a red diamond in each panel of Figure 5.

In comparing the behavior of the ionospheric height measurements over the Northeastern (Fig. 6a) and Southeastern U.S. (Fig. 6b) with IRI-estimated heights, we see similar findings over time. The D-region-measured ionospheric heights rise more quickly than IRI at the beginning of the night, and remain higher longer as morning approaches. In both cases, there is also a downward dip in measured ionospheric heights at dawn, along with an increased spread in the measurements. The limited D-region measurements in the Indian sector (Fig. 6c) during the dawn terminator also show this dawn-related dip and spread in the estimated heights. Possible causes for this dip will be discussed below.

While daytime D-region measurements are scarce due to lightning activity, where the data exist, there is fairly good agreement between IRI and the D-region measurements in this paper. India and Japan (Fig. 6c,d) have good measurements covering the 11:00-18:00 LT and 12:00-17:00 LT sectors, respectively. Northeastern U.S. and Southeastern U.S. have good daytime coverage of 6:00-10:00 LT and 15:00 – 18:00 UT. The daytime trend for all the D-region measurements show IRI under-estimating ionospheric height just after dawn, through about

10:00 LT. After 10:00 LT to dusk, IRI ionospheric heights are in good agreement with the D-region measurements.

The blue solid line at the bottom of each panel shows a histogram of lightning counts within 200 km of any probed grid cell with 10-minute bin size. All lightning histograms are on the same scale, shown on the righthand ordinate axis, with the maximum number of counts being 6600 (reached in the Southeastern U.S. region). High lightning activity within 200 km indicates that the ionospheric region that is probed by this technique could be affected by electric fields in the thunderstorm itself (Shao et al., 2013; Lay et al., 2014). Given that we chose this date because of a significant storm in the U.S. to demonstrate the technique, it is not surprising that the number of lightning events near the ionospheric measurement locations is high. However, there are some periods where the majority of lightning activity is more than 200 km away from the probed region, indicating that the measured ionosphere is not likely to be directly electrically affected by thunderstorms, although it could be affected by distantly-produced gravity waves. For example, the measured ionosphere during the time period of 00:00 – 08:00 LT in the Northeastern U.S. has very little nearby electrical activity. There is relatively little lightning activity within 200 km in Japan and India, indicating that the probed ionosphere is more likely to be in a quiet state (unperturbed by local lightning activity). These considerations are important in comparisons to IRI, since IRI does not include tropospheric conditions as input. We will discuss implications of tropospheric effects below.

4. Discussion and Summary

This paper demonstrates how the ENTLN lightning location and waveform measurements can be used to probe the D-region ionosphere globally. While this technique is limited to regions with lightning activity and good coverage of ENTLN stations, the areas that meet these criteria are much more ubiquitous than regions that are currently able to be measured by existing D-region techniques. We hope to expand global D-region measurements using this technique to get a better understanding of global variations in the D-region ionosphere. In this paper we show that the waveform behavior from ENTLN measurements is consistent with predicted behavior from the work of Shao and Jacobson (2009) regarding waveform shape and station-to-receiver distance. We also show that the diurnal behavior of the D-region effective ionospheric height is observable with this technique. In addition, variation with time scales of 30 minutes to several hours is observed with several kilometers change in reflection height. These magnitudes and time scales are consistent with previously-observed D-region perturbations near thunderstorms (Lay and Shao, 2011a,b). This technique has the potential to monitor longer-term trends in D-region behavior on a global scale, as well as to monitor impacts of atmospheric gravity wave activity on the global lower ionosphere.

Given that D-region measurements for validation are sparse, we use the International Reference Ionosphere (IRI) D-region model for comparison. This is an empirical model based on fewer than 30 rocket flights. We find that the general diurnal variation in IRI agrees well with our model, but there are significant differences in the sharpness of the rise in ionospheric

height near the beginning of the nighttime ionosphere, and the fall-off in ionospheric height in the morning is delayed from IRI, and sharper. Previous findings using this LF/VLF lightning probing technique with the LASA ground-based lightning array (Lay et al, 2014) found that nighttime ionospheres over thunderstorms were generally higher than nighttime ionospheres over quiet areas, so that could be part of the reason for the increased height over IRI. However, longer-term monitoring of D-region behavior using this technique could help determine if the steep increase in height at the beginning of the night and then relatively flat level throughout the night, as seen in the U.S. in this case, is a general trend or driven primarily by thunderstorm activity. In addition, daily tropospheric conditions are not accounted for in IRI, so gravity wave effects are not predicted.

The dawn terminator also shows an interesting feature in all three regions with data during this local time (Southeastern U.S., Northeastern U.S., and India): a sudden and significant spread in ionospheric heights as well as a significant dip in height to nearly mid-day values that then recovers after about an hour to a more moderate decrease in height that better corresponds with IRI. This apparent change in height could be due to an unaccounted-for change in waveform shape from complex ray bending at the terminator, or it could be a real change in height. Jacobson et al. (2008) showed a significant asymmetry between dawn-dusk VLF reflectivity off the D-region ionosphere, with more energy absorbed in the 5-50 kHz frequency range from the dawn terminator than the dusk terminator. It is possible that this frequency-dependent absorption of energy distorts the expected waveform shape and results in an error in estimated ionospheric height. This feature will be studied in more depth in future work.

Long-term monitoring of the D-region ionosphere using this technique could be especially beneficial for constraining and validating D-region models. By looking at many different dates with this technique, one could look at differences in D-region behavior in latitude, especially near the equator, where very few D-region measurements have been made. The particular day chosen for this study did not have much equatorial and Southern Hemispheric lightning due to it being in May. Recent work by DiGangi et al. (2022) has shown excellent ENTLN coverage in South America, indicating future studies of the D-region in South America may be beneficial.

Acknowledgements

This work was funded by Defense Advanced Research Projects Agency (DARPA) AtmoSense program. The authors would like to thank Advanced Environmental Monitoring (AEM) for providing the Earth Networks Total Lightning Network data.

Data Availability

Earth Networks Total Lightning Network location and waveform data can be requested at https://www.earthnetworks.com/product/lightning-data/.

References

Astafyeva, E. (2019). Ionospheric detection of natural hazards. *Rev. of Geophysics*, *57*(4), 1265-1288. https://doi.org/10.1029/2019RG000668

Bilitza, D., Pezzopane, M., Truhlik, et al. (2022). The International Reference Ionosphere model: A review and description of an ionospheric benchmark. *Rev. of Geophys., 60*, e2022RG000792. https://doi.org/10.1029/2022RG000792

Cheng, Z., S. A. Cummer, H.-T. Su et al. (2007), Broadband very low frequency measurement of D region ionospheric perturbations caused by lightning electromagnetic pulses, *J. Geophys. Res., 112*, A06318. https://doi.org/10.1029/2006JA011840

Cohen, M. B., Gross, N. C., Higginson-Rollins, M. A. et al. (2018). The lower ionospheric VLF/LF response to the 2017 Great American Solar Eclipse observed across the continent. *Geophys. Res. Lett.*, *45*(8), 3348-3355. https://doi.org/10.1002/2018GL077351

Cummer, S. A., Inan, U. S., & Bell, T. F. (1998). Ionospheric D region remote sensing using VLF radio atmospherics. *Rad. Sci.*, *33*(6), 1781-1792.

Dellinger, J.H. (1937), Sudden Disturbances of the Ionosphere, *Proceedings of the Institute of Radio Engineers, Volume 25, Number 10.* https://doi.org/10.1109/JRPROC.1937.228657

DiGangi, E., J. Lapierre, M. Stock et al. (2022), Analyzing lightning characteristics in central and southern South America, *Electric Power Systems Research*, *213*, 108704. https://doi.org/10.1016/j.epsr.2022.108704

Ferguson, J. A., and F. P. Snyder (1987), The segmented waveguide program for long wavelength propagation calculations, Tech. Doc. No. 1071, Nav. Ocean Syst. Cent., San Diego, Calif.

Friedrich, M., Pock, C., & Torkar, K. (2018). FIRI-2018, an updated empirical model of the lower ionosphere. Journal of Geophysical Research: Space Physics, 123, 6737–6751. https://doi.org/10.1029/2018JA025437

Friedrich, M., & Torkar, K. M. (2001). FIRI: A semiempirical model of the lower ionosphere. *J. of Geophys. Res., 106*(A10), 21, 409–21, 418. https://doi.org/10.1029/2001JA900070

Frissell, N. A., Vega, J. S., Markowitz, E. et al. (2019). High-frequency communications response to solar activity in September 2017 as observed by amateur radio networks. *Space Weather, 17*, 118–132. https://doi.org/10.1029/2018SW002008

Galvan, D. A., A. Komjathy, M. P. Hickey et al. (2012), Ionospheric signatures of Tōhoku-Oki tsunami of March 11, 2011: Model comparisons near the epicenter, *Rad. Sci., 47*, RS4003. https://doi.org/10.1029/2012RS005023

Jacobson, A. R., R. H. Holzworth, and X.-M. Shao (2008), Low-frequency ionospheric sounding with narrow bipolar event lightning radio emissions: Energy-reflectivity spectrum, *Ann. Geophys., 26*, 1793–1803. https://doi.org/10.5194/angeo-26-1793-2008

Kelley, M. C. (2009). *The Earth's ionosphere: Plasma physics and electrodynamics*. Academic press. Oxford, U.K.

Laby, T. H., J. J. McNeill, F. G. Nicholls, and A. F. B. Nickson (1940), Waveform, energy and reflexion by the ionosphere, of atmospherics, *Proc. R. Soc. A*, 174, 145–163

Lay, E. H. (2018). Ionospheric irregularities and acoustic/gravity wave activity above low-latitude thunderstorms. *Geophys. Res. Lett., 45*. https://doi.org/10.1002/2017GL076058

Lay, E. H., X.-M. Shao, A. K. Kendrick et al. (2015), Ionospheric acoustic and gravity waves associated with midlatitude thunderstorms, *J. Geophys. Res. Space Physics, 120*. https://doi.org/10.1002/2015JA021334

Lay, E. H., X.-M. Shao, and A. R. Jacobson (2014), D region electron profiles observed with substantial spatial and temporal change near thunderstorms, *J. Geophys. Res. Space Physics*, 119. https://doi.org/10.1002/2013JA019430

Lay, E. H., and X.-M.Shao (2011b), Multi-station probing of thunderstorm-generated D-layer fluctuations by using time-domain lightning waveforms, *Geophys. Res. Lett.,38*, L23806. https://doi.org/10.1029/2011GL049790

Lay, E. H., and X.-M. Shao (2011a), High temporal and spatial-resolution detection of D-layer fluctuations by using time-domain lightning waveforms, *J. Geophys. Res., 116*, A01317. https://doi.org/10.1029/2010JA016018

Liu, C., & Heckman, S. (2011). The application of total lightning detection and cell tracking for severe weather prediction. 91st American Meteorological Society Annual Meeting, Seattle.

Marshall, R. A., & Snively, J. B. (2014). Very low frequency subionospheric remote sensing of thunderstorm-driven acoustic waves in the lower ionosphere. *J. Geophys. Res.: Atmospheres*, *119*(9), 5037-5045. https://doi.org/10.1002/2014JD021594

McCormick, J. C., Cohen, M. B., Gross, N. C. et al. (2018). Spatial and temporal ionospheric monitoring using broadband sferic measurements. *J. of Geophys. Res.: Space Physics, 123*, 3111–3130. https://doi.org/10.1002/2017JA024291

McDonald III, T. B, Uman, M. A., Tiller, J. A., et al. (1979). Lightning Location and Lower-Ionospheric Height Determination From Two-station Magnetic Field Measurements. *J. of Geophys. Res.: Oceans, 84*(C4), 1727–1734, https://doi.org/10.1029/JC084iC04p01727

Schunk, R., & Nagy, A. (2000). *Ionospheres: physics, plasma physics, and chemistry*. Cambridge university press. Cambridge, U.K.

Shao, X. M., Lay, E. H., & Jacobson, A. R. (2013). Reduction of electron density in the night-time lower ionosphere in response to a thunderstorm. *Nature Geoscience*, *6*(1), 29-33. https://doi.org/10.1038/ngeo1668

Shao, X.-M., and A. R. Jacobson (2009), Model simulation of very low frequency and low frequency lightning signal propagation over intermediate ranges, *IEEE Trans. Electromagn. Compat., 51*, 519–525. https://doi.org/10.1109/TEMC.2009.2022171

Thomson, N. R. (1993), Experimental daytime VLF ionospheric parameters, *J. Atmos. Terr. Phys., 55*(2), 173–184.

Wait, J. R., and K. P. Spies (1964), Characteristics of the Earth-Ionosphere Waveguide for VLF Radio Waves, Tech. Notes 300, Natl. Bur. of Standards, Washington, D. C.

Zhu, Y., Rakov, V. A., Tran, M. D. et al. (2017). Evaluation of ENTLN performance characteristics based on the ground truth natural and rocket-triggered lightning data acquired in Florida. *J. of Geophys. Res.: Atmos., 122*. 9858–9866. https://doi.org/10.1002/2017JD027270

Figure Captions

Figure 1. a) Schematic of signal propagation geometry. Ground wave travels directly from source to station, ionospheric wave reflects off ionosphere and then arrives at station. b) Raw ENTLN digitizer counts from a lightning time waveform that occurred on 01 May 2017 at 02:10:03 UT at 29.08^{o}N, 89.14^{o}W, measured at a distance of 540 km by station CLVSN, with irregular time sampling (black dots) and interpolated to 1-μs time sampling (black line). c)

Normalized E-field waveform determined from the raw digitizer waveform using Equation 2. Δt is the time difference between trough of ground wave and peak of ionospheric reflection.

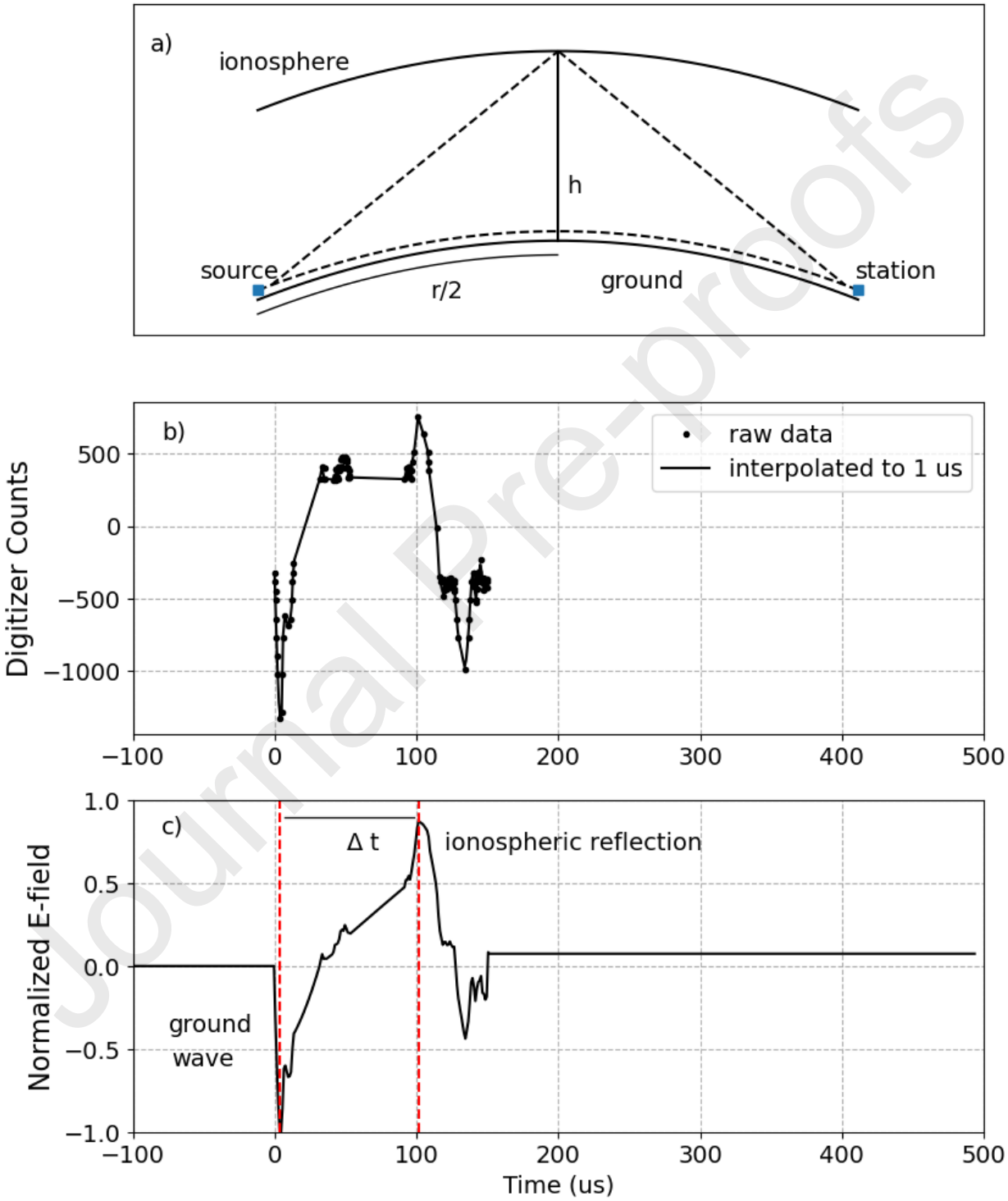

Figure 2. a) Map of Southeastern U.S. region of interest with ENTLN lightning activity from 00:00 – 10:00 UTC on 1 May 2017. Colorbar represents lightning UTC. Blue squares show ENTLN stations. Red square highlights station PLMCH. b) Time waveforms detected at PLMCH between 00:00 – 02:00 UTC, averaged in 50-km distance bins (vertical axis). N shows the number of individual waveforms contributing to each average.

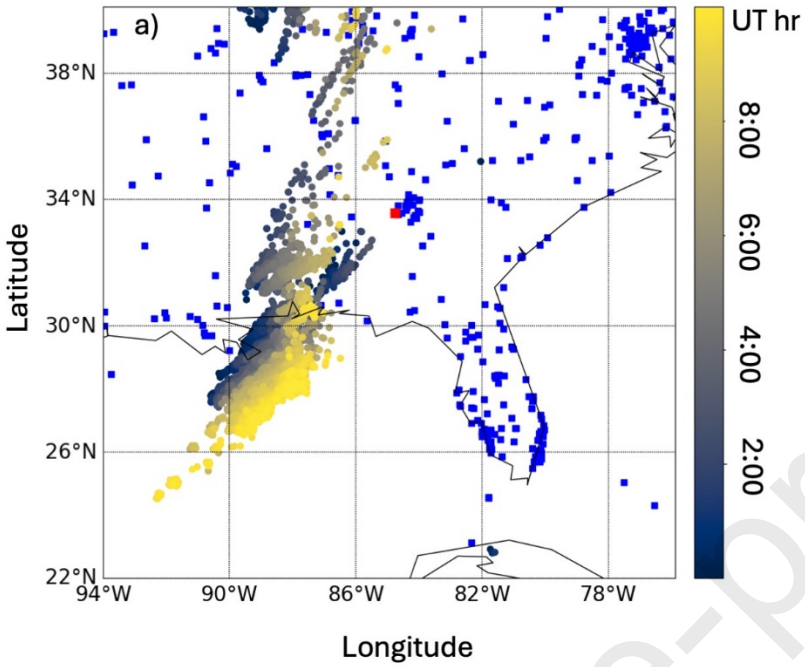

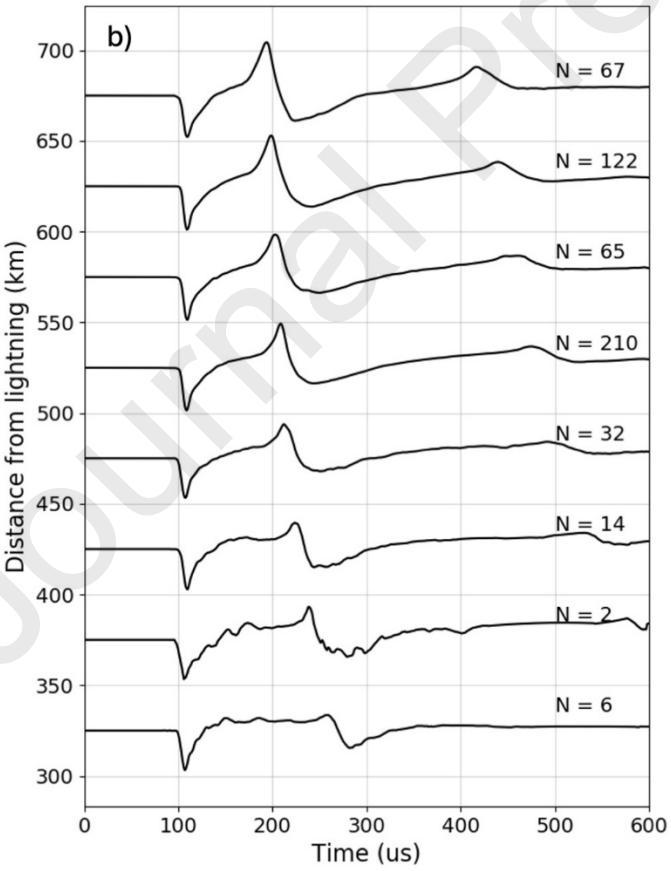

Figure 3. Colored dots show measured effective ionospheric height in local time, with 00:00 at local midnight on 1 May 2017. Colorbar shows distance from lightning to station of each measurement. Black line shows 30-minute median of measurements. White squares show the height where IRI plasma frequency equals 100 kHz.

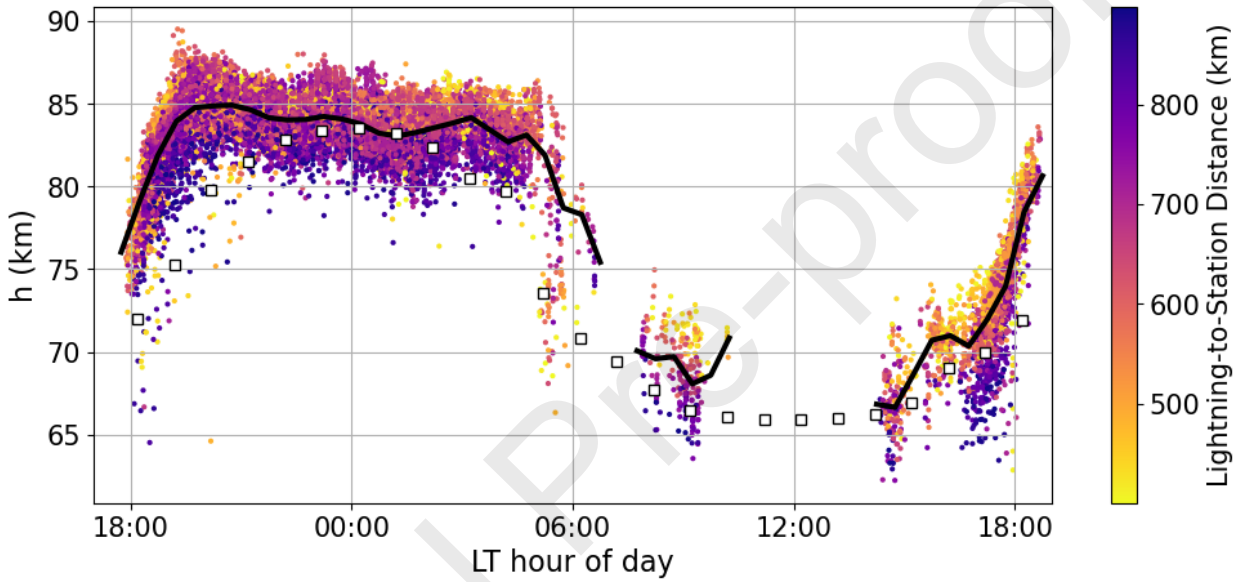

Figure 4. a) Gray dots show ionospheric probed locations (midpoint between lightning and station) during 01:00-10:00 UT in Southeastern U.S. Black rectangles highlight 6 regions of interest used in righthand panels. b-g) Fluctuations in effective height of the probed midpoints in each of the 6 regions during local nighttime. Color represents number of measurements in each 0.5 km x 10-min cell, from 1 (yellow) to 45 (dark blue). Solid line represents median in time. Dashed lines represent standard deviation.

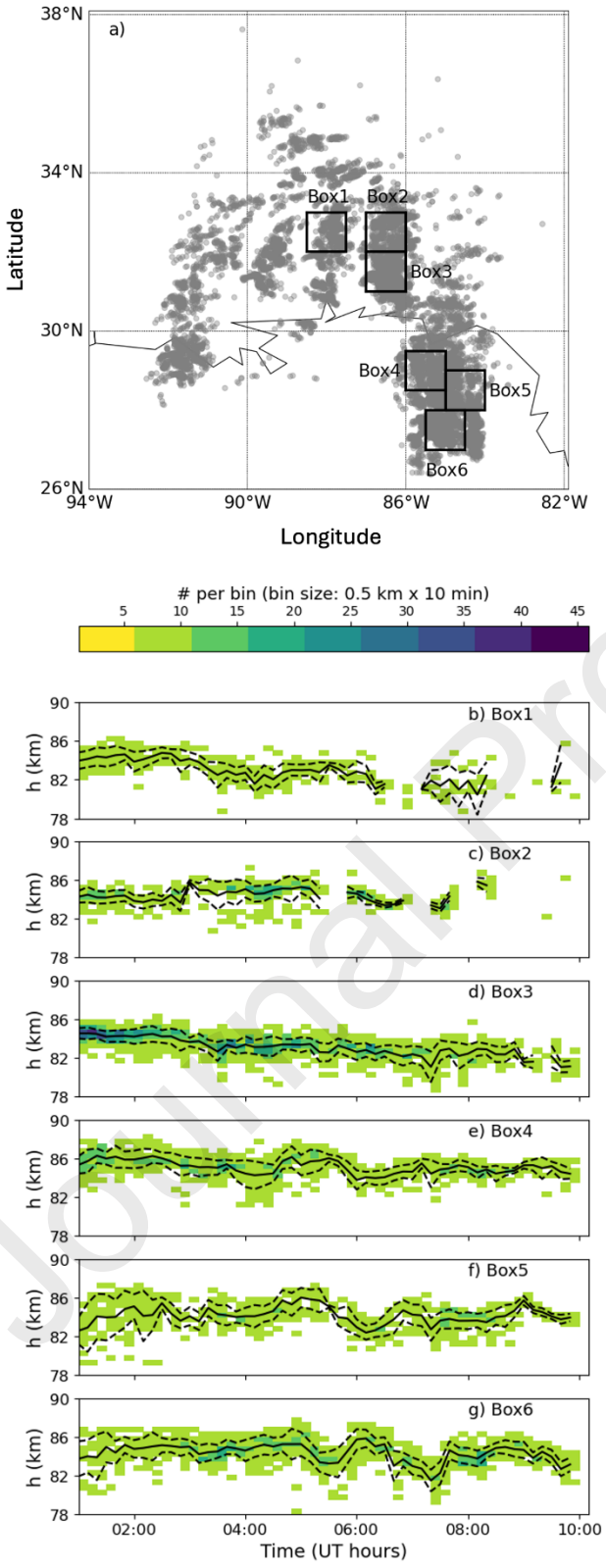

Figure 5. Four global regions of interest used in Figure 6 and associated results. Colored dots show ENTLN lightning locations in UTC (colorbar). Blue squares show ENTLN receivers. Red diamond shows location of IRI model run for each region.

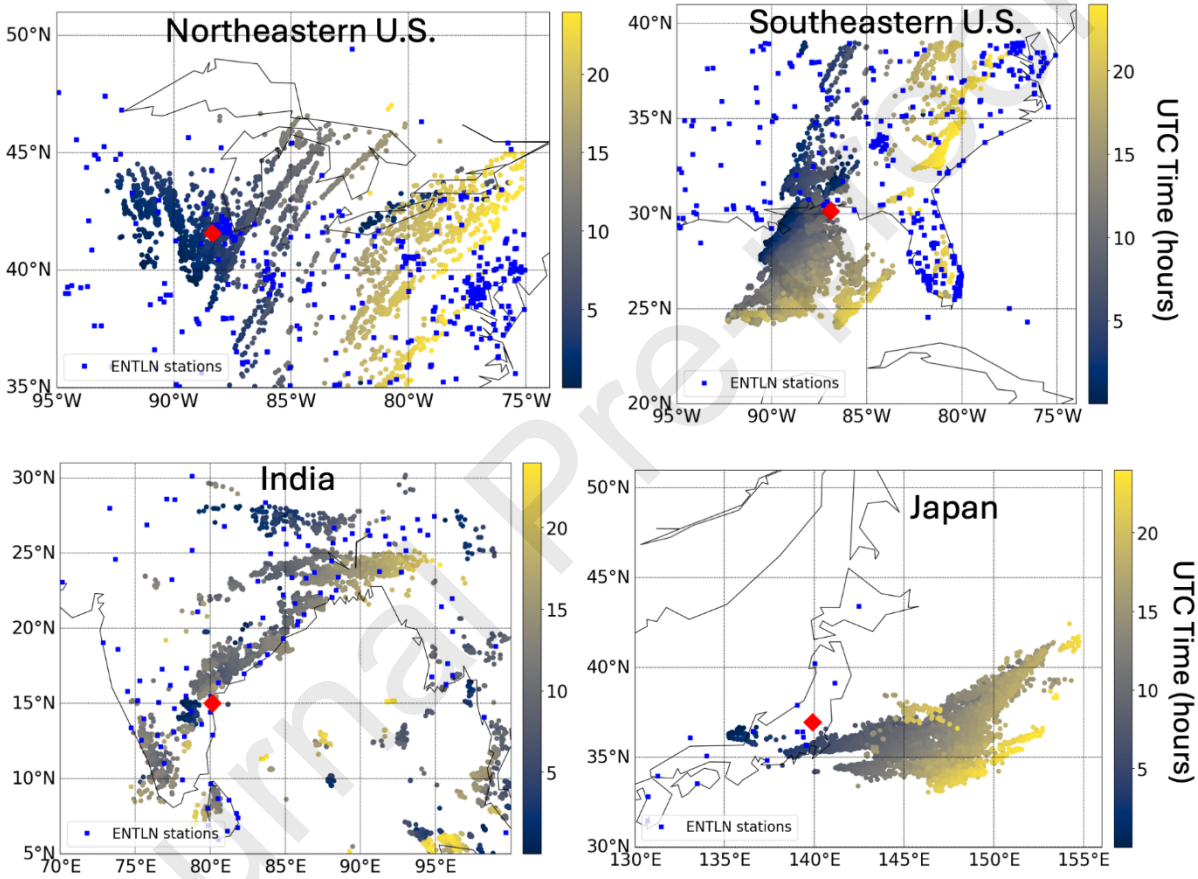

Figure 6. Measured effective ionospheric height in the 4 regions shown in Figure 5. All data are from 00:00 – 23:59 UTC on 1 May 2017, but they have been shifted by regional longitude to show their local time behavior. Gray dots show effective height measurements, black lines show the 30-minute median of those measurements. Blue squares show hourly IRI model runs, where plasma density equals 100 kHz. Thin blue lines show how many lightning events occurred within 200 km of the probed D-region areas, in 10-minute bins.

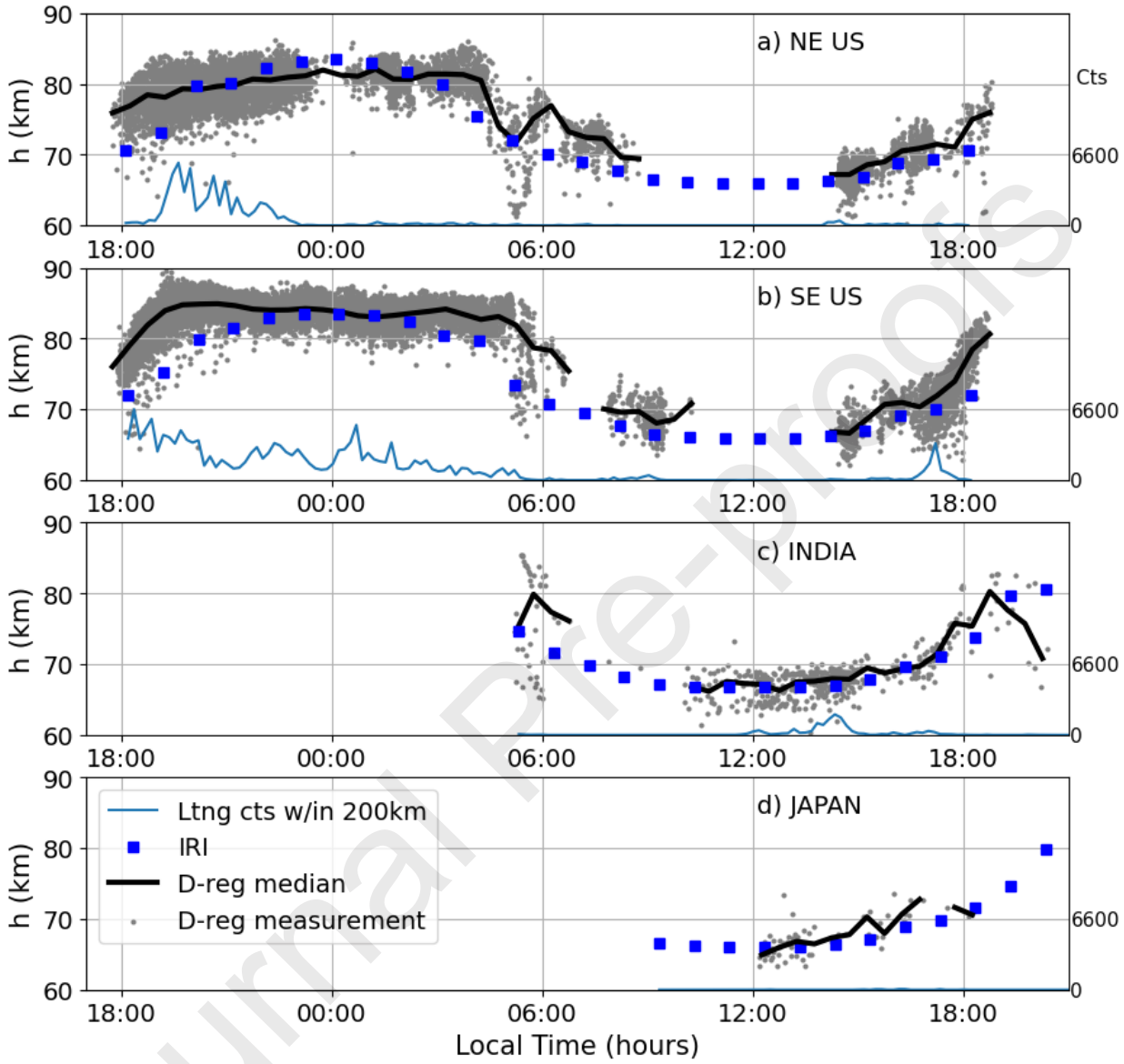

Declaration of Interest Statement

The authors of the submitted work, “Probing the D-region ionosphere globally with Earth Networks Total Lightning Network data”, have no financial or personal relationships to declare.

Erin Lay

Emily Hudson

Danielle Markowski

Xuan-Min Shao

Todd Anderson